Hindawi
Advances in Condensed Matter Physics
Volume 2021, Article ID 2370816, 9 pages
https://doi.org/10.1155/2021/2370816

Research Article

Density Functional Theory Study on the Effect of Isomorphic Substitution of FAU Molecular Sieve on N_2 Adsorption Performance

Mengya Wang,[1,2,3] Rong Cao,[1,2,3] Jiezhen Xia,[1,2,3] Luchao Zhao,[1,2,3] Yong Li,[1,2] Qimi Ciren,[4] Dongye Zhao,[1,2] Shifeng Wang,[1,2,3] Chun Du ,[1,3] and Qi Wu [1,2,3]

[1]*Department of Physics, School of Science, Tibet University, Lhasa 850000, China*
[2]*Institute of Oxygen Supply, Center of Tibetan Studies (Everest Research Institute), Tibet University, Lhasa 850000, China*
[3]*Key Laboratory of Cosmic Rays (Tibet University), Ministry of Education, Lhasa 850000, China*
[4]*Tibet Autonomous Region Energy Research Demonstration Center, Lhasa 850000, China*

Correspondence should be addressed to Chun Du; duchun@utibet.edu.cn and Qi Wu; wuqi_zangda@163.com

Received 8 September 2021; Accepted 7 October 2021; Published 22 October 2021

Academic Editor: Shuyuan Xiao

Low pressure and anoxia are the main characteristics of the environment in the Tibetan Plateau, which means people living there have a large demand for oxygen to reduce the symptoms of altitude sickness. Pressure swing adsorption (PSA) is a competitive oxygen production technology in plateau areas, which relies on the molecular sieves for the separation of N_2 and O_2 in industry and portable medical equipment. The adsorption characteristics of the Faujasite-type (FAU) molecular sieves, as one kind of the most widely used adsorbents for O_2 production, depend on the properties, amount, and distribution of the skeleton cations and atoms. In this paper, we explore the isomorphic substitution effect on the adsorption properties of N_2 in FAU molecular sieves using the computational approaches based on the density functional theory (DFT). The structural analysis and adsorption energy calculated for the Zn, Ca, and Ga substitutions at the Si/Al skeleton sites in the β-cage structure, the basic unit of FAU molecular sieves, prove that the isomorphic substitution effect can strengthen the adsorption of N_2. The Bader charge and density of states analysis validate the formation of electron-deficient holes near the Fermi level and hence strengthen the local polarity of the pore structure and enhance the adsorption of N_2 molecules. The work about isomorphic substitution on the FAU molecular sieves might provide an insight into heteroatom isomorphic modification mechanisms and designing excellent air separation materials.

1. Introduction

The plateau area of China accounts for more than one quarter of the total area of country and has an important strategic military affairs status [1]. The air pressure in Qinghai Tibet Plateau is low (i.e., the air pressure at 5500 m is half less than that in plain area) and the temperature difference between day and night is large. Hypobaric hypoxia has become the main characteristic of plateau environment [1]. According to the relevant research of neuroimaging, high-altitude environment will have a significant impact on the human brain [1]. Hypoxia can cause vomiting, fever, dizziness, and other different symptoms [2]. Therefore, in order to ensure the survival of people in these areas, there is a great requirement for oxygen (O_2) [3]. Research shows that, in oxygen-enriched environment, it can significantly reduce altitude reaction and sleep difficulty [4]. Therefore, it is very important to create an oxygen-enriched environment to effectively improve cognitive function [5].

The method of separating oxygen (O_2) and nitrogen (N_2) from air has aroused widespread interest in the pharmaceutical and chemical industries. Conventionally, the oxygen production technologies can be classified into physical oxygen production and chemical oxygen production methods. The physical methods of oxygen production are mainly air

separation, distillation, and compression (including pressure swing adsorption, membrane separation, and low-temperature distillation). Chemical oxygen production methods include water electrolysis, superoxide, and sodium chlorate oxygen candles. Pressure swing adsorption (PSA) technology using specific adsorbents is very competitive in the realization of air oxygen enrichment [6–8]. This method has many advantages, such as short start-up time, handy start-up and end-up, low energy expenditure, and low cost [9–11]. In view of the special oxygen demand in plateau areas such as China's Qinghai Tibet Plateau, some experts pointed out that PSA is the most economical and suitable technology. Pressure swing adsorption technology is based on the molecular characteristics of gas components and affinity for adsorption materials, under pressure to separate some gas components from the gas mixture technology. The process was carried out at a temperature close to the ambient temperature. Under high pressure, adsorbent is used to adsorb target gas. The common adsorbents are zeolite molecular sieves, activated carbon, and other special adsorption materials. Then, in order to desorb the adsorbed material, the process turns to low pressure.

Pressure swing adsorption (PSA) technology can realize the separation of O_2 on a lesser scale. Adsorbents are very important for PSA in industry and portable medical equipment. Generally speaking, in air separation, two types of the common adsorption processes were divided. The first process is to use zeolite molecular sieves as nitrogen adsorbent under the conditions of equilibrium. Oxygen is a process product because the quadrupole moment of nitrogen is higher than that of oxygen. The second method is to use carbon molecular sieves (CMSs) as oxygen adsorbents. Zeolite molecular sieves are a kind of major inorganic crystal materials extensively used in chemical industry, catalyst, adsorbent, ion exchange, and other fields. In air separation, because the quadrupole moment of nitrogen is higher than that of oxygen and the force between cation and N_2 in the adsorbent is greater than O_2, the equilibrium adsorption capacity of N_2 is higher than that of O_2. Therefore, zeolite molecular sieve can selectively adsorb nitrogen rather than oxygen and provide oxygen close to pure oxygen. Molecular sieve is a three-dimensional framework structure with ordered micropores with diameter of 2 nm. It has a variety of structures. The main reason is that the T atoms (tetrahedron) in the lattice have different connection ways. The common T atoms are silicon and aluminum. Zeolite molecular sieves have the advantages of low cost, high stability, and easy ion exchange. At the same time, they can adjust the gas-solid interaction by selecting the appropriate ratio of silicon to aluminum. The Linde type-A (LTA) and Faujasite-type (FAU) molecular sieves are the most widely used adsorbents for O_2 production [12, 13]. Due to the large temperature difference in plateau environment, FAU molecular sieves usually have higher N_2–O_2 selectivity than LTA molecular sieves in PSA process. FAU molecular sieves are composed of Si, Al, and O atoms, and their crystal composition changes with the change of Si/Al ratio. FAU molecular sieves are composed of sodalite gabions connected by hexagonal prism. Their properties depend on the properties, amount, and distribution of the skeleton cations and atoms. Ion exchange modification [14], dealumination modification [15], heteroatom isomorphic replacement modification, and pore modification [16] can change the structure of molecular sieves and affect their performance.

Heteroatom isomorphic substitution modification can introduce specific nonmetal or metal atoms into the original framework of molecular sieves to change the redox performance and catalytic activity of molecular sieves and avoid the possible problems of loss of active species and blockage of micropores by nonframework species [17]. Isomorphic substitution refers to the substitution of the T atom (tetrahedron) in the molecular sieves lattice [18]. The isomorphic substitution modification method is widely used in ZSM-5 [19], SBA-15 [20], UTL [21], and other kinds of molecular sieves. The commonly used metals in this modification include Zn [19], Ga [22], Ca [19, 23], Fe [19, 21], and Cr [18, 24]. Among them, the metals Zn, Ca, and Ga have been widely used in the modification of molecular sieves. For example, El-Malki et al. [25] introduced Zn, Ga, and Fe into the HZSM-5 cavity to study acidic sites through sublimation. The study found that, after sublimation, the concentration of Bronsted acid site is low, but, for Ga/ZSM-5 and Fe/ZSM-5, it increases again after hydrolysis. Miyake et al. [26] studied the direct and selective conversion of methanol to para-xylene over the zinc ion-doped ZSM-5/silica molecular sieve-1 core-shell zeolite catalyst. The study found that the p-xylene yield of this catalyst was 40.7 C-mol%, and the para-selectivity was higher than 99 C-mol%. Li et al. [27] used calcium doped biosilica to control bleeding and found that Ca-biosilica is expected to be a fast hemostatic agent due to its effectiveness, excellent biocompatibility, and simple and environmentally friendly preparation process. Liu et al. [28] studied Ga-doped ZSM-22 zeolite as a highly selective and stable catalyst for the isomerization of n-dodecane. The study found that Ga-substituted zeolite has high crystallinity, uniform morphology, and open pore structure. Similar to the zeolites discussed above, Al and Si atoms in FAU molecular sieves can also be replaced by metals. Although a lot of studies have been done on the properties of isomorphic substituted molecular sieves, we still do not know much about how to change the structure and electronic properties of framework atoms after the introduction of heteroatoms, so as to affect their adsorption properties. In particular, there are few reports on nitrogen adsorption in isomorphic FAU molecular sieves, and it is necessary to study FAU molecular sieves as an important catalyst for air separation.

In this work, the energetics of Zn, Ca, and Ga substitution for Si/Al skeleton atoms in FAU molecular sieves have been investigated based on the density functional theory (DFT), by predicting the substituting effect on the adsorption properties of N_2 molecule. We introduce the metal atoms of Zn, Ca, and Ga into β-cage structure which is the basic unit of FAU molecular sieves. Our simulated results reveal that the pore structure has different degrees of relaxation when the skeleton atoms are replaced by metal atoms of Zn, Ca, and Ga; and the isomorphic substitution of skeleton atoms can enhance the adsorption of N_2 molecule.

Our work aims to explore the substitution effect and modification mechanism of isomorphic substitution of metal atoms from the perspective of theoretical prediction, so as to improve the adsorption activity of molecular sieves. This theoretical arithmetic based on computational science has turned out to be a feasible and efficient method to achieve this goal. In addition, we hope that our results can provide guidance for further experimental research in the field of molecular sieves.

2. Calculation Method and Theoretical Models

Density functional theory (DFT) is calculated by using the plane-wave basis in the Vienna ab initio simulation package (VASP) [29]. The core and valence electrons were treated by the projector augmented plane-wave (PAW) method [30]. The generalized gradient approximation (GGA) with the Perdew-Burke-Ernzerhof (PBE) functional was used to represent the exchange-correlation energy [31]. The van der Waals (vdW) interaction is described by using the DFT-D3 method for all calculations. All atoms were fully optimized until the magnitude of the Hellmann-Feynman force and energy on every atom converged to less than 0.2 eV/Å and 10^{-5} eV, respectively. The cutoff energy was set to 400 eV for the plane-wave basis set. The Brillouin zone (BZ) was sampled by a Monkhorst-Pack $1 \times 1 \times 1$ k-point sampling grid for the β-cage structures.

The lattice constant of the FAU molecular sieve structure model was $a = b = c = 25.028$ Å, belonging to Fd3m space group of hexagonal system. As shown in Figure 1(a), the structural unit of the FAU skeleton was the β-cage. Adjacent β-cages were connected by hexagonal columns to form a system of holes and cavities. The holes and cavities are formed by silicon oxygen tetrahedrons and aluminum oxygen tetrahedrons, which are connected by oxygen bridge bonds. Due to the limited computational resources, the β-cage structure of the FAU structural unit (Figure 1(b)) was intercepted from the whole FAU framework in the calculation. The β-cage structure contains 24 Al atoms, 24 Si atoms, and 72 O atoms, making it a multielectron system with nonzero charge. Through analysis, the Si, Al, and O Bader charges were 1.73, 0.62, and 7.63$|e|$, respectively. As Figure 1(c) shows, the Al atoms lose outer electrons, and Si and O atoms have electron localization.

The N_2 molecular adsorption energy (E_{ads}) is calculated as follows:

$$E_{\text{ads}} = E_{N_2/\text{FAU}} - E_{\text{FAU}} - E_{N_2}, \tag{1}$$

where E_{ads} represents the adsorption energy, $E_{N_2/\text{FAU}}$ is the total energy after the adsorption of N_2 molecules in the β-cage channel of FAU, E_{FAU} is the total energy of the intercepted β-cage, and E_{N_2} is the energy of N_2.

3. Results and Discussions

3.1. Structural Properties. To study the effect of isomorphic substitution on the adsorption properties of FAU molecular sieves, Zn, Ca, and Ga atoms were used to replace the Al or Si atoms in the β-cage of FAU molecular sieves, respectively. The β-cage structure is composed of eight-membered rings and twelve-membered rings containing Si-O-Al. There are two kinds of Al and Si skeleton atoms at different positions, as shown in the dotted box in Figure 1(b). One kind contains Al and Si atoms that connect with two eight-membered rings, and the other kind contains Al′ and Si′ atoms that connect with the eight-membered rings and twelve-membered rings. The Zn, Ca, and Ga atoms are incorporated into the β-cage and replace the two kinds of Al and Si atoms, respectively. The optimized structures of the Zn, Ca, and Ga substitutions of the Al and Si atoms in the β-cage are shown in Figures 2(a)~2(f), and the optimized structures of the substitution of Al′ and Si′ atoms are shown in Figures 2(g)~2(l). Therefore, in our simulations, we totally considered twelve hybrid structures and calculated their formation energies. Among all the hybrid structures, only three doping systems, that is, Zn-doping (Al), Ca-doping (Al), and Ca-doping (Si), have the negative formation energies of −4.12 eV, −1.22 eV, and −3.14 eV, respectively. The results indicate that the Zn and Ca atoms tend to substitute the skeleton Al atom; in contrast, the Ga atom is more easily to replace the skeleton Si atom. Hence, these three hybrid structures and the pristine β-cage were adopted in the following simulations for the adsorption properties analysis.

To manifest the structural changes before and after introducing Zn, Ca, and Ga in the framework of the β-cage, the root mean square (RMS) displacement formula was used to calculate the structural relaxation of the substitution position (Al/Si/Al′/Si′). The RMS displacement was calculated as follows:

$$r_{\text{RMS}} = \sqrt{\frac{1}{3}\sum_{i=1}^{3}\left(r_i - r_i^0\right)^2}, \tag{2}$$

where r_i^0 and r_i are the bond lengths of Al/Si-O in the undoped structure and Al/Si/Zn/Ca/Ga-O in the doped structure, respectively.

The calculated RMS displacement is shown in Table 1. Combined with Figure 2, it can be seen that the pore structure has different degrees of relaxation after the skeleton atoms (Al/Si/Al′/Si′) are replaced by Zn, Ca, and Ga atoms. It shows that doping will have a certain effect on the structure.

3.2. Adsorption Properties for the Pristine β-Cage. Four adsorption structures and adsorption energies of N_2 at β-cage channels were calculated. The calculated adsorption energy results are shown in Table 2. One can see from the table that the adsorption energies of the four sites are −0.69 eV, −0.49 eV, −0.44 eV, and −0.78 eV. The simulated results mean that N_2 can be adsorbed at the four adsorption sites with relatively small adsorption energies and low adsorption capacity. Figure 3 depicts the optimization model and the charge differential density diagram of N_2 adsorbed on the pristine β-cage. According to the RMS displacement displayed in Table 2, N_2 can be adsorbed in the β-cage channel, leading to very tiny structural relaxation in the pore. Based

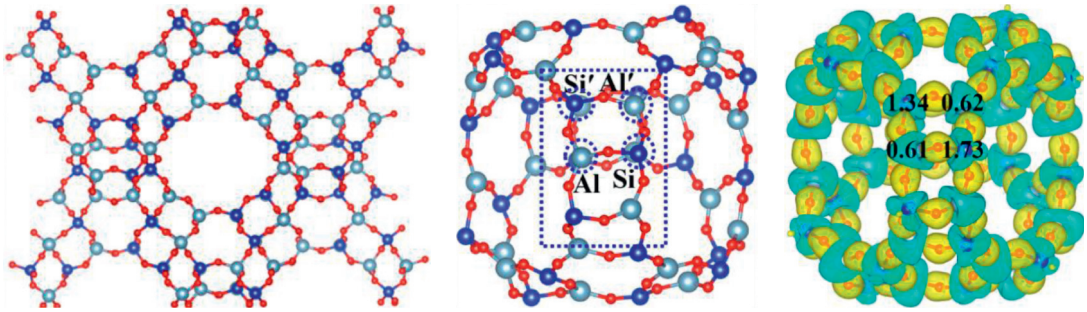

Figure 1: (a) Structure of the FAU molecular sieves. (b) Structure of the β-cage. (c) Charge difference diagram of β-cage. The isosurface value is 0.002 e Bohr^{-3}. The cyan part represents an increase in charge density, and the yellow part represents a decrease in charge density. Red, dark blue, and light blue represent the O, Al, and Si atoms.

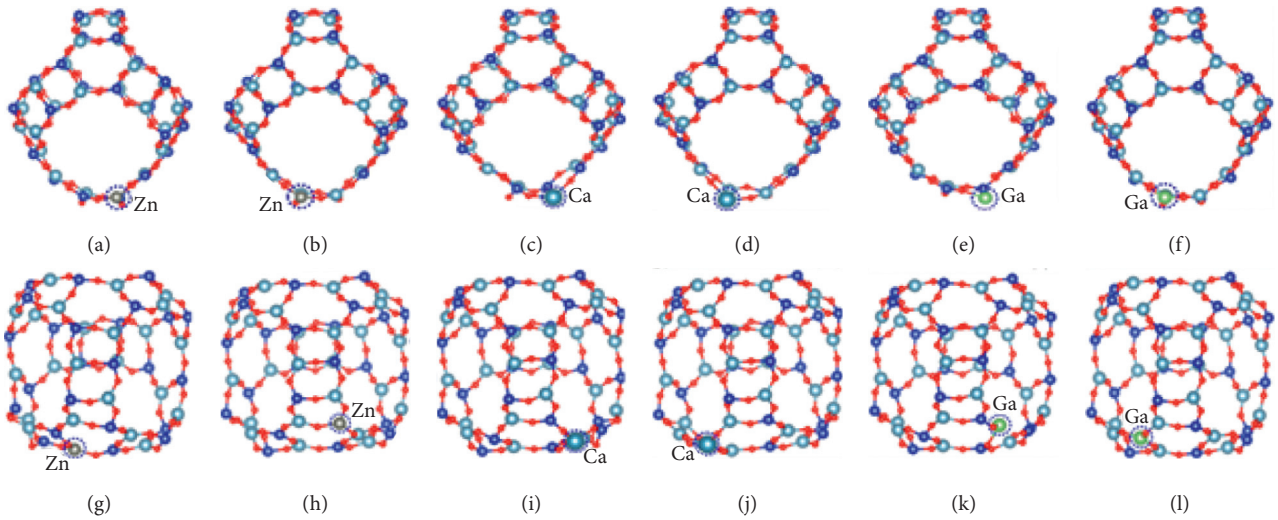

Figure 2: Structure diagrams of Zn, Ca, and Ga substitutions at Al, Si, Al′, and Si′. (a, c, e) Zn/Ca/Ga substitutions at Al site; (b, d, f) Zn/Ca/Ga substitutions at Si site; (g, i, k) Zn/Ca/Ga substitutions at Al′ site; (h, j, l) Zn/Ca/Ga substitutions at Si′ site.

Table 1: Calculated lattice constants, lengths of Al/Si/Zn/Ca/Ga-O bonds, and r_{RMS} of the different substituted atoms in the Zn/Ca/Ga-doped β-cage and pristine β-cage after optimization.

	Lattice constants/Å	Bond length (Si-O)/Å	Bond length (Al-O)/Å	Bond length (Zn/Ca/Ga–O)/Å	r_{RMS}/Å
Pristine (Al, Si)	25.028	1.661	1.706	—	—
Pristine (Al′, Si′)	25.028	1.618	1.721	—	—
Zn-doping (Al)	25.028	1.601	1.747	1.880	0.11
Zn-doping (Al′)	25.028	1.625	1.762	1.911	0.12
Zn-doping (Si)	25.028	1.585	1.757	1.913	0.15
Zn-doping (Si′)	25.028	1.602	1.750	1.912	0.18
Ca-doping (Al)	25.028	1.591	1.736	2.150	0.26
Ca-doping (Al′)	25.028	1.623	1.770	2.181	0.27
Ca-doping (Si)	25.028	1.645	1.715	2.213	0.32
Ca-doping (Si′)	25.028	1.577	1.778	2.190	0.34
Ga-doping (Al)	25.028	1.604	1.725	2.238	0.31
Ga-doping (Al′)	25.028	1.607	1.715	2.130	0.24
Ga-doping (Si)	25.028	1.635	1.708	1.788	0.08
Ga-doping (Si′)	25.028	1.657	1.710	1.785	0.10

on the Bader charge analysis, the average valence charges for the four skeleton atoms (Al/Al′/Si/Si′) are 0.61 eV, 0.62 eV, 1.73 eV, and 1.34 eV, respectively. After interaction with the N_2 molecule, the corresponding average valence charges for the four skeleton sites (Al/Al′/Si/Si′) change to 0.58 eV, 0.62 eV, 1.61 eV, and 1.43 eV, exhibiting that there is no

Table 2: Calculated lengths of the Al/Si-O bonds and r_{RMS} and E_{ads} before and after N_2 adsorption at the Al/Si/Al′/Si′ sites of the pristine β-cage.

Adsorption Site	Bond length (Al/Si-O)/Å (before adsorption)	Bond length (Al/Si-O)/Å (after adsorption)	r_{RMS}/Å	E_{ads}/eV
Pristine (Al)	1.661 1.706 1.706	1.641 1.704 1.701	0.012	-0.69
Pristine (Al′)	1.618 1.721 1.721	1.673 1.688 1.770	0.047	-0.49
Pristine (Si)	1.661 1.706 1.661	1.647 1.705 1.645	0.012	-0.44
Pristine (Si′)	1.618 1.721 1.618	1.672 1.698 1.602	0.035	-0.78

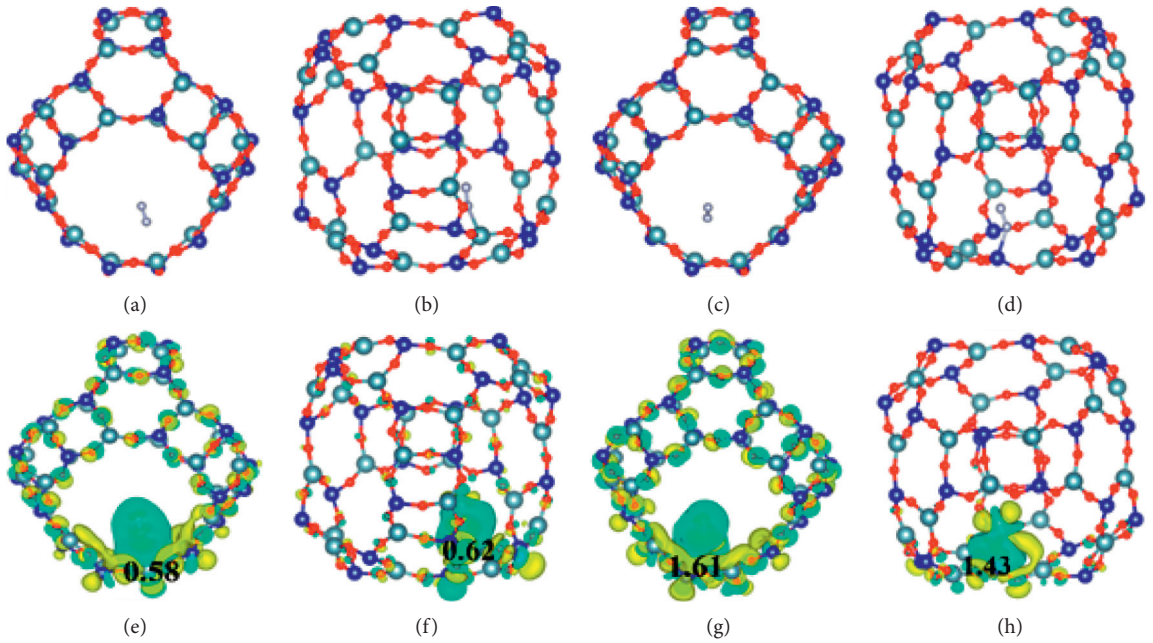

Figure 3: Adsorption structure and charge differential density diagram of N_2 adsorbed at the β-cage. Al (a, e), Al′ (b, f), Si (c, g), and Si′ (d, h) sites. The average valence charge of the adsorption site is shown in the figure; the isosurface value is 0.002 e $Bohr^{-3}$.

obvious charge transfer between the adsorption sites with N_2.

3.3. Adsorption Properties after Isomorphic Substitution. To reveal the effect of doping on N_2 adsorption, the adsorption energies of N_2 at the adsorption sites of the β-cage were calculated. We systematically considered five adsorption sites, containing the metal sites (Zn, Ca, and Ga) and their adjacent Al/Si and Al′/Si′ sites for each heteroatom doped structure and hence totally fifteen adsorption sites were simulated for the N_2 adsorption. All the stable optimized model and adsorption energies are provided in Figure 4 and Table 3, respectively. Other doped structures are not considered because the adsorption energy is very small and even close to zero. As Table 3 shows, the most stable adsorbable structure is based on the model of Zn and Ca substitutions at Al site and a Ga isomorphic substitution for Si atom. The adsorption centers are the Zn, Ca, and Ga heteroatoms and adjacent Al, Al′, Si and Si′ atoms. As seen, only six structures can adsorb the N_2 molecules with a negative adsorption energy: Zn substituting Al atoms, Ca substituting Al atoms, and Ga substituting Si atoms. For the structure with the isomorphic substitution of Al atoms with Zn, N_2 cannot be adsorbed at the Zn heteroatom site and the adjacent Al′ and Si′ sites with a very large and positive adsorption energy. In the case of the isomorphic substitution of Al atoms with Ca, only the Al′ site can adsorb N_2, while the other sites cannot adsorb N_2. When introducing Ga atoms into the β-cage, the N_2 molecule can be adsorbed at the Si, Si′, and Al′ sites near Ga atoms.

Compared with the pristine β-cage structure, the absorption energies of N_2 molecule are much larger for the isomorphic substitution of Si/Al atoms with the metal atoms Zn/Ca/Ga. Our calculated results reveal that the isomorphic substitution of the framework atoms by the metal atoms results in a much stronger interaction between the N_2 molecule and also the β-cage structure. The structure containing the isomorphic substitution of Zn for Al atoms has the largest absorption energy when N_2 is adsorbed at the Si site near the Zn atom. The charge differential density results reveal that there is obvious charge transfer between N_2 and the adsorption sites. Compared with Figure 3, the charge transferring between the Al′ and Si′ sites is relatively local due to a certain extent relaxation of the pore structure after metal atoms doping.

3.4. Electronic Structure Analysis. The projected density of states (PDOS) properties for the adsorption sites were

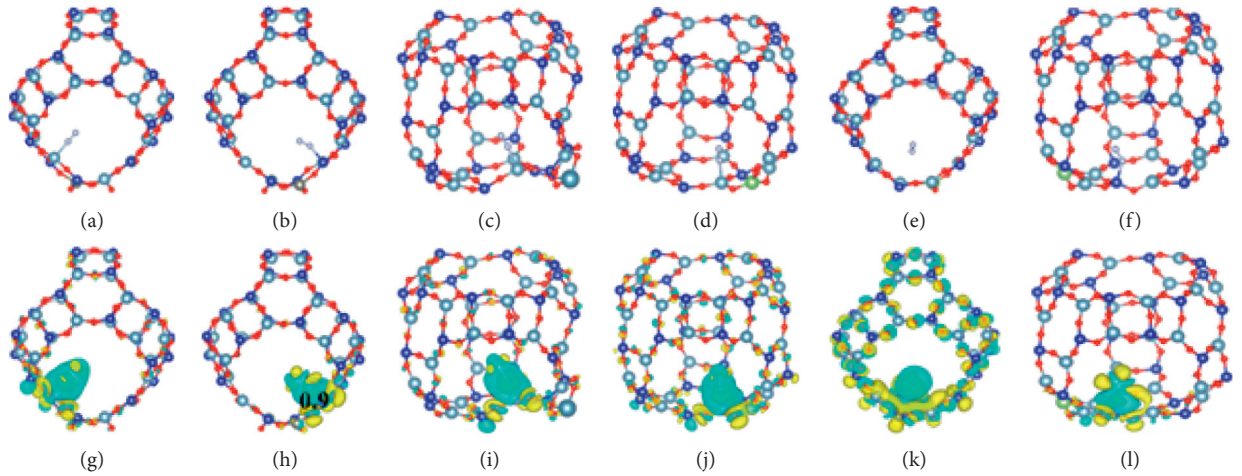

Figure 4: Structure models and charge difference density diagrams of N_2 adsorption at three kinds of doped β-cages that are optimized as the best adsorption sites: (a, g) Zn replaces Al (Al), (b, h) Zn replaces Al (Si), (c, i) Ca replaces Al (Al′), (d, j) Ga replaces Si (Al′), (e, k) Ga replaces Si (Si), and (f, l) Ga replaces Si (Si′). The average valence charge of the Si site after N_2 adsorption is shown in the figure; the isosurface value is 0.002 e $Bohr^{-3}$.

Table 3: Calculated lengths of Al/Si-O bonds and r_{RMS} and E_{ads} of N_2 adsorption at the Al/Si/Al′/Si′ sites of the doped β-cage.

Doping type	Adsorption site	Bond length (Al/Si/-O)/Å (before adsorption)	Bond length (Al/Si/-O)/Å (after adsorption)	r_{RMS}/Å	E_{ads}/eV
Zn-doping (Al)	Al (Zn)	1.601 1.747 1.737	1.651 1.774 1.748	0.033	−1.31
	Si (Zn)	1.601 1.747 1.590	1.648 1.764 1.608	0.031	−1.91
Ca-doping (Al)	Al′ (Ca)	1.650 1.767 1.736	1.713 1.721 1.743	0.042	−1.06
	Al′ (Ga)	1.635 1.708 1.708	1.643 1.704 1.715.	0.007	−1.14
Ga-doping (Si)	Si (Ga)	1.642 1.708 1.635	1.639 1.702 1.639	0.003	−0.83
	Si′ (Ga)	1.635 1.708 1.642	1.650 1.704 1.610	0.021	−0.94

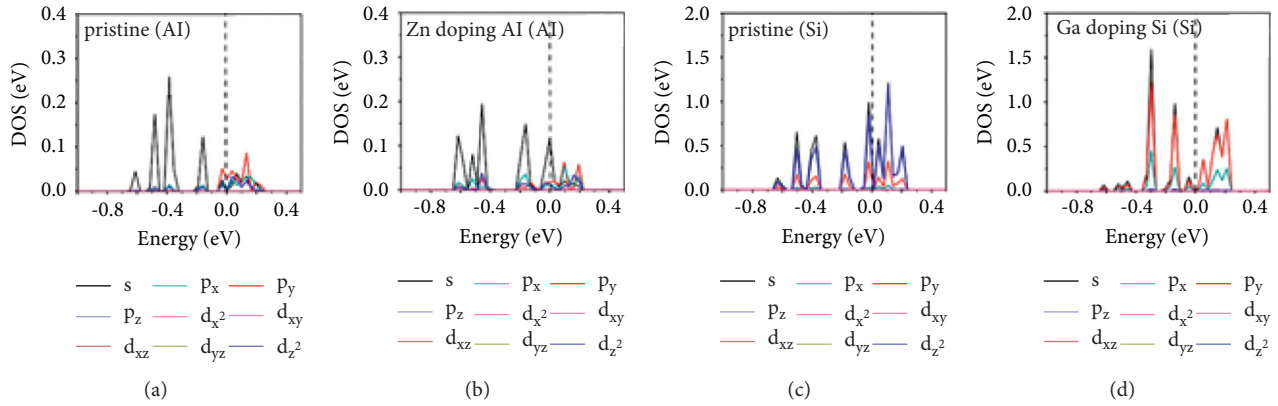

Figure 5: Continued.

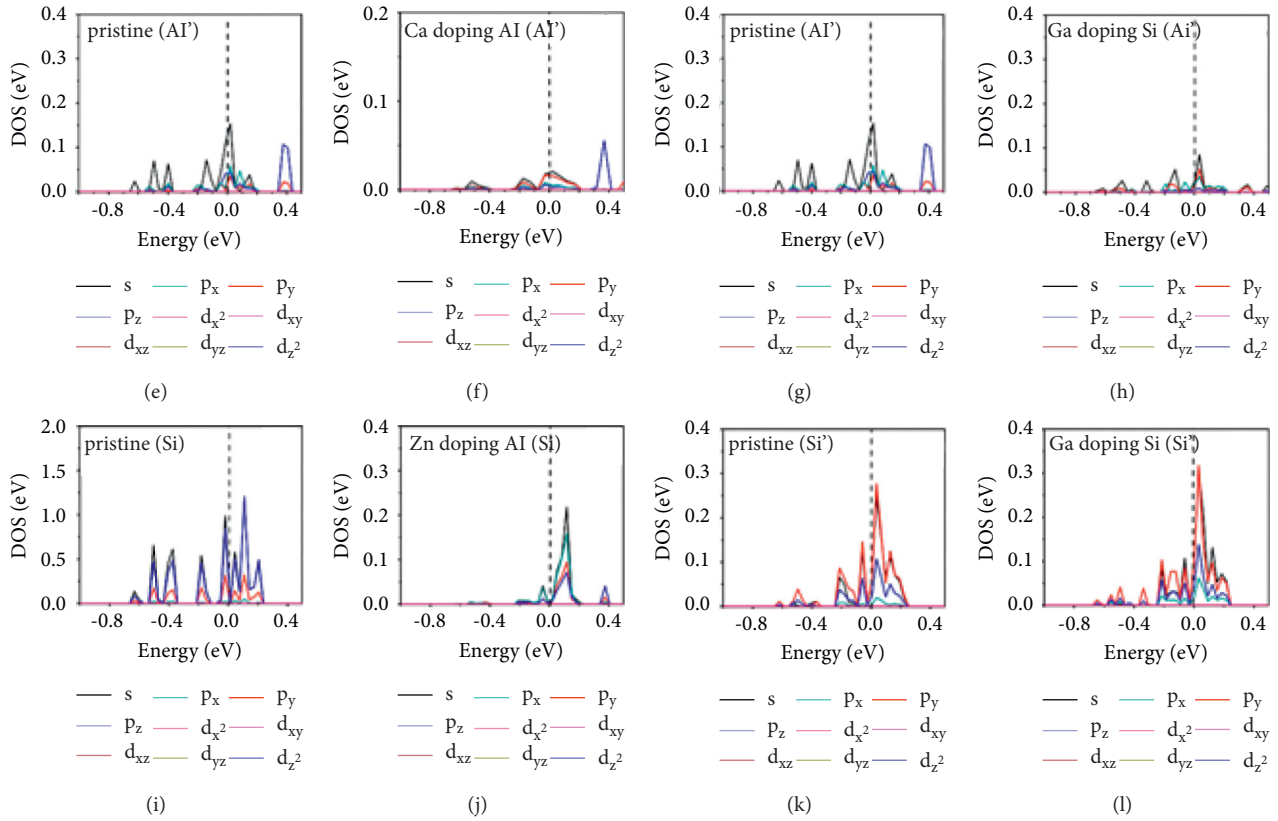

FIGURE 5: The projected density of states (PDOS) for the adsorption sites (Al/Al′/Si/Si′ atoms) in the pure β-cage and the relative adsorption sites in the Zn/Ca/Ga-doped β-cage. The dashed line shows the Fermi level.

calculated in order to comprehensively explore the substitution effect on the adsorption properties of β-cage structure. Figure 5 shows the density of states of the all the stable structures after N_2 adsorption. Compared with the DOS plots of the four adsorption sites on the pristine β-cage structure (Figures 5(a), 5(c), 5(e), 5(g), 5(i), and 5(k)), the density of states of all the adsorbable structures (Figures 5(b), 5(d), 5(f), 5(j), 5(h), and 5(l)) has significant changes. The DOS analysis results show that the number of electronic states near the Fermi level significantly decreases. As for metal materials, we know that the higher the electron density near the Fermi level is, the more active the free electrons it has. For the Zn-doped β-cage pore structure, the N_2 molecule on the adjacent Si atom has the largest adsorption energy. As Figure 5(d) shows, the number of electronic states for the Si site near the Fermi level almost decreases to zero. The Bader charge analysis of Zn-doping is calculated, which shows that the charge of the Si site decreases from 1.61 eV to 0.9 eV, forming electron-deficient holes. This result is attributed to the electron loss in the pore framework structure after Al^{3+} is replaced by Zn^{2+}, since the coordination of the metals does not match the substituted atoms. Therefore, Zn-doping leads to the formation of electron-deficient holes near Si sites as the electronic structure analysis results exhibit and thus enhances the local polarity of the pore structure and enhances the adsorption of N_2 molecules.

4. Conclusion

In summary, we introduce Zn, Ca, and Ga dopants into the FAU basic unit β-cage channel structure to activate the basal skeleton structure for air separation. Detailed calculations are carried out for the pristine β-cage and the Zn, Ca, and Ga substitutions at the skeleton Si/Al sites, which lead to the following conclusions: (1) The results showed that all the adsorption sites in the pure β-cage channel were very weak, especially for the Si site. The relative adsorption energy was only 0.44 eV. (2) The isomorphic substitution of Zn, Ca, and Ga on the pristine β-cage structure greatly enhances the adsorption of N_2 molecule. This is because electron loss appeared in the pore framework structure after the skeleton Si/Al atom was replaced by Zn/Ca/Ga, since the coordination of the metals does not match the substituted atoms. Therefore, the incorporation of Zn/Ca/Ga into the β-cage leads to the formation of electron-deficient holes at the adsorption sites and thus enhances the local polarity of the pore structure and enhances the adsorption of N_2 molecules. In the absence of relevant background, these findings provide molecular understanding, such as the influence of different heteroatom distribution, different adsorption structure, and other factors on the adsorption process and properties.

Data Availability

The data used to support the findings of this study are included within the article.

Conflicts of Interest

The authors declare that they have no conflicts of interest.

Acknowledgments

This work was financially supported by the National Natural Science Foundation of China (Grant no. 22168036) and Department of Education of Tibet Autonomous Region ([2021]1-21 Theoretical research and design of two dimensional electrocatalytic materials).

References

[1] X. Wei, X. Ni, S. Zhao, and A. Chi, "Influence of exposure at different altitudes on the executive function of plateau soldiers-evidence from ERPs and neural oscillations," *Frontiers in Physiology*, vol. 12, Article ID 632058, 2021.

[2] A. M. Luks, E. R. Swenson, and P. Bärtsch, "Acute high-altitude sickness," *European Respiratory Review*, vol. 26, no. 143, Article ID 160096, 2017.

[3] Y. Fu, Y. Liu, Z. Li et al., "Insights into adsorption separation of N_2/O_2 mixture on FAU zeolites under plateau special conditions: a molecular simulation study," *Separation and Purification Technology*, vol. 251, 2020.

[4] A. M. Luks, H. van Melick, R. R. Batarse, F. L. Powell, I. Grant, and J. B. West, "Room oxygen enrichment improves sleep and subsequent day-time performance at high altitude," *Respiration Physiology*, vol. 113, no. 3, pp. 247–258, 1998.

[5] Y. Liu, Z. Song, C. Song, and D. Wang, "A novel point source oxygen supply method for sleeping environment improvement at high altitudes," *Building Simulation*, vol. 14, pp. 1–18, 2021.

[6] S. P. Reynolds, A. D. Ebner, and J. A. Ritter, "Enriching PSA cycle for the production of nitrogen from air," *Industrial & Engineering Chemistry Research*, vol. 45, no. 9, pp. 3256–3264, 2006.

[7] J. C. Santos, P. Cruz, T. Regala, F. D. Magalhães, and A. Mendes, "High-purity oxygen production by pressure swing adsorption," *Industrial & Engineering Chemistry Research*, vol. 46, no. 2, pp. 591–599, 2007.

[8] A. M. M. Mendes, C. A. V. Costa, and A. E. Rodrigues, "Oxygen separation from air by PSA: modelling and experimental results: Part I: isothermal operation," *Separation and Purification Technology*, vol. 24, no. 1-2, pp. 173–188, 2001.

[9] R. S. Todd and P. A. Webley, "Pressure drop in a packed bed under nonadsorbing and adsorbing conditions," *Industrial & Engineering Chemistry Research*, vol. 44, no. 18, pp. 7234–7241, 2005.

[10] D.-K. Moon, Y. Park, S.-H. Kim, M. Oh, and C.-H. Lee, "Analysis of thermal parameter effects on an adsorption bed for purification and bulk separation," *Separation and Purification Technology*, vol. 181, pp. 95–106, 2017.

[11] A. M. Ribeiro, J. C. Santos, and A. E. Rodrigues, "PSA design for stoichiometric adjustment of bio-syngas for methanol production and co-capture of carbon dioxide," *Chemical Engineering Journal*, vol. 163, no. 3, pp. 355–363, 2010.

[12] W. Loewenstein, "The distribution of aluminum in the tetrahedra of silicates and aluminates," *American Mineralogist*, vol. 39, pp. 92–97, 1954.

[13] S. Calero, D. Dubbeldam, R. Krishna et al., "Understanding the role of sodium during adsorption. A force field for alkanes in sodium exchanged faujasites," *Journal of the American Chemical Society*, vol. 126, no. 36, pp. 11377–11386, 2004.

[14] X. Sheng, Y. Zhou, Y. Duan, Y. Zhang, and M. Xue, "Effect of different lanthanum source and preparation method on the lanthanum-doped mesoporous SBA-15 synthesis," *Journal of Porous Materials*, vol. 18, no. 6, pp. 677–683, 2011.

[15] W. T. Lim, S. M. Seo, O. S. Lee, L. Wang, and G. Q. Lu, "Synthesis and crystal structure of dehydrated, deaminated, and dealuminated zeolite Y (FAU): single-crystal structure of $|Na_{33}\ H_{26}\ (Al_5\ O_4\ )|[Si_{126}\ Al_{66}\ O_{384}\ ]$-FAU," *Journal of Inclusion Phenomena and Macrocyclic Chemistry*, vol. 67, no. 3-4, pp. 261–269, 2010.

[16] L. Tao, G.-S. Li, S.-F. Yin et al., "Synthesis and characterization of H-ZSM-5 zeolites and their catalytic performance in CH_3Br conversion to aromatics," *Reaction Kinetics, Mechanisms and Catalysis*, vol. 103, no. 1, pp. 191–207, 2011.

[17] G. Wang, H. Yuan, A. Kuang, W. Hu, G. Zhang, and H. Chen, "High-capacity hydrogen storage in Li-decorated $(AlN)_n$ ($n = 12, 24, 36$) nanocages," *International Journal of Hydrogen Energy*, vol. 39, no. 8, pp. 3780–3789, 2014.

[18] S. Ahmed, "Methanol to olefins conversion over metal containing MFI-type zeolites," *Journal of Porous Materials*, vol. 19, no. 1, pp. 111–117, 2011.

[19] K. Omata, Y. Yamazaki, Y. Watanabe, K. Kodama, and M. Yamada, "Artificial neural network (ANN)-aided optimization of ZSM-5 catalyst for the dimethyl ether to olefin (DTO) reaction from neat dimethyl ether (DME)," *Industrial & Engineering Chemistry Research*, vol. 48, no. 13, pp. 6256–6261, 2009.

[20] J. Ma, L.-S. Qiang, J.-F. Wang, X.-B. Tang, and D.-Y. Tang, "Effect of different synthesis methods on the structural and catalytic performance of SBA-15 modified by aluminum," *Journal of Porous Materials*, vol. 18, no. 5, pp. 607–614, 2010.

[21] M. V. Shamzhy, O. V. Shvets, M. V. Opanasenko et al., "Synthesis of isomorphously substituted extra-large pore UTL zeolites," *Journal of Materials Chemistry*, vol. 22, no. 31, p. 15793, 2012.

[22] X. Su, G. Wang, X. Bai et al., "Synthesis of nanosized HZSM-5 zeolites isomorphously substituted by gallium and their catalytic performance in the aromatization," *Chemical Engineering Journal*, vol. 293, pp. 365–375, 2016.

[23] R. Kawase, A. Iida, Y. Kubota et al., "Hydrothermal synthesis of calcium and boron containing MFI-type zeolites by using organic amine as structure directing agent," *Industrial & Engineering Chemistry Research*, vol. 46, no. 4, pp. 1091–1098, 2007.

[24] G. Wang, H. Chen, Y. Li, A. Kuang, H. Yuan, and G. Wu, "A hybrid density functional study on the visible light photocatalytic activity of (Mo,Cr)-N codoped $KNbO_3$," *Physical Chemistry Chemical Physics*, vol. 17, no. 43, pp. 28743–28753, 2015.

[25] E.-M. El-Malki, R. A. van Santen, and W. M. H. Sachtler, "Introduction of Zn, Ga, and Fe into HZSM-5 cavities by sublimation: identification of acid sites," *The Journal of Physical Chemistry B*, vol. 103, no. 22, pp. 4611–4622, 1999.

[26] K. Miyake, Y. Hirota, K. Ono, Y. Uchida, S. Tanaka, and N. Nishiyama, "Direct and selective conversion of methanol to para-xylene over Zn ion doped ZSM-5/silicalite-1 core-

shell zeolite catalyst," *Journal of Catalysis*, vol. 342, pp. 63–66, 2016.

[27] J. Li, J. Han, Q. Sun et al., "Biosynthetic calcium-doped biosilica with multiple hemostatic properties for hemorrhage control," *Journal of Materials Chemistry B*, vol. 6, no. 47, pp. 7834–7841, 2018.

[28] S. Liu, Y. He, H. Zhang et al., "Design and synthesis of Ga-doped ZSM-22 zeolites as highly selective and stable catalysts forn-dodecane isomerization," *Catalysis Science & Technology*, vol. 9, no. 11, pp. 2812–2827, 2019.

[29] G. Kresse and J. Furthmüller, "Efficient iterative schemes for ab initio total-energy calculations using a plane-wave basis set," *Physical Review B*, vol. 54, no. 16, pp. 11169–11186, 1996.

[30] G. Kresse and D. Joubert, "From ultrasoft pseudopotentials to the projector augmented-wave method," *Physical Review B*, vol. 59, no. 3, pp. 1758–1775, 1999.

[31] J. P. Perdew, K. Burke, and M. Ernzerhof, "Generalized gradient approximation made simple," *Physical Review Letters*, vol. 77, no. 18, pp. 3865–3868, 1996.